Catalysis Science & Technology

Accepted Manuscript

ROYAL SOCIETY OF CHEMISTRY

www.rsc.org/catalysis

Catalysis Science & Technology

Catalysis Science & Technology

Dynamic Article Links ►

Cite this: DOI: 10.1039/c0xx00000x

ARTICLE TYPE

www.rsc.org/xxxxxx

A comparative study of PdZSM-5, Pdβ, and PdY in hybrid catalyst for syngas to hydrocarbons

Chun Wang[a,b], Xiangang Ma[a] , Qingjie Ge[a,*] and Hengyong Xu[a,*]

Received (in XXX, XXX) Xth XXXXXXXXX 20XX, Accepted Xth XXXXXXXXX 20XX

DOI: 10.1039/b000000x

Catalytic conversion of syngas into hydrocarbons over hybrid catalyst consisting of methanol synthesis catalyst and Pd modified zeolite (PdZSM-5, Pdβ, and PdY) was investigated. The results indicate that the intermediate dehydration step of DME in syngas to hydrocarbon process mainly happens on the Brönsted acid sites of the Pd zeolite. The large pores and cavities of Pdβ and PdY promote the formation of C_4+ hydrocarbons, which are mainly gasoline-type branched hydrocarbons. Moreover, the large pores and cavities provide enough space for the formation of higher aromatics which are the precursor of coke. The blockage of micropores in Pd-zeolite by hydrocarbon-type coke results in the deactivation of hybrid catalysts.

Introduction

It is well-known that petrochemicals are mainly produced from oil refineries. With the depletion of petroleum resources, synthesis of petrochemicals from other resources becomes more attractive. Syngas can be produced from various non-petroleum resources such as natural gas, biomass and other carbonaceous materials including coal, recycled plastics and municipal wastes[1, 2]. Thus, developing a syngas to hydrocarbon process can effectively reduce the consumption of petroleum resources.

There are two typical routes for producing hydrocarbons from syngas: Fischer-Tropsch synthesis (FTS)[3-5] and syngas-to-hydrocarbons via methanol/dimethyl ether (DME)[6-8]. The FTS process usually gives a wide carbon number distribution of hydrocarbons due to the limitation of Anderson-Schulz-Flory (ASF) polymerization kinetics[9]. Many efforts have been made to increase the selectivity to fractions within a certain range by designing novel catalysts, such as core-shell structured catalyst[10] and mesoporous zeolite supported catalyst[11, 12]. However, it was reported that the formed methane (CH_4) from secondary cracking was relatively high. Compared with the FTS process, the syngas-to-hydrocarbons via methanol/DME process could selectively achieve hydrocarbons with different cuts while keeping the methane selectivity low[8, 13, 14]. The process had been realized in producing liquefied petroleum gas (LPG, C_3 and C_4 alkanes)[14-16], aromatic hydrocarbon mixtures[17] and gasoline fractions[8, 18]. The hybrid catalyst usually consists of two components: a methanol synthesis catalyst and a zeolite or metal modified zeolite. Syngas was first converted into methanol over a methanol synthesis catalyst, and then to hydrocarbons over a zeolite or metal modified zeolite. For example, syngas could be selectively converted into LPG over a hybrid catalyst composed of Cu-ZnO-Al_2O_3 methanol synthesis catalyst (CZA) and PdY[14] while the major product became gasoline over CZA/PdZSM-5[18]. Such combination could break the thermodynamic equilibrium limitation of methanol synthesis due to the in situ removal of methanol. In addition, the modification of Pd in Pd modified zeolite was found to promote the stability of the hybrid catalyst as well as the formation of saturated hydrocarbons[8, 18]. Herein, we have carried out a comparative study around syngas conversion over hybrid catalysts containing different types of Pd modified zeolites: PdZSM-5, Pdβ and PdY, with similar SiO_2/Al_2O_3 ratios. All these zeolites were modified with Pd by ion-exchange methods and then physically mixed with Cu-ZnO-Al_2O_3 methanol synthesis catalyst to form a hybrid catalyst. Catalyst coke analysis was investigated by TPO-MS and N_2-Physical adsorption techniques.

Experimental

1. Catalyst preparation

Parent HZSM-5(SiO_2:Al_2O_3=23), Hβ (SiO_2:Al_2O_3=25) and HY (SiO_2:Al_2O_3=30) were purchased from Zeolyst International. CuO-ZnO-Al_2O_3 catalyst (CZA) powder and γ-Al_2O_3 (197.4 m^2/g) powder were mixed uniformly at a weight ratio of 9:5 to form DME synthesis catalyst. The DME synthesis catalyst was crushed into 20-40 mesh and denoted as CZAA. The prepared CZAA showed excellent performance for DME synthesis in our previous work[8].

Pd modified HZSM-5(SiO_2:Al_2O_3=23), Hβ (SiO_2:Al_2O_3=25), and HY (SiO_2:Al_2O_3=30) were prepared by ion-exchange methods while the theoretical loading of Pd in Pd modified zeolite was 0.5 wt%. After washing with deionized water, the Pd modified zeolite catalysts were dried at 120°C for 4 hrs and calcined at 550°C for 4 hrs. Finally, the Pd modified zeolite catalysts were crushed into particles of 20-40 mesh and denoted as PdZSM-5, Pdβ, and PdY, respectively. Cu-ZnO-Al_2O_3 catalyst (CZA) and Pd modified zeolite were physically mixed together at a weight ratio of 1:1 to form the hybrid catalyst. The

hybrid catalysts were denoted as CZA/PdZSM-5, CZA/Pdβ, CZA/PdY and CZA/γ-Al_2O_3, respectively.

2. Catalyst test

A pressurized flow type reaction apparatus with a fixed bed reactor was used for this study. The fixed bed reaction system consisted of a 12 mm inner diameter tubular reactor and an electronic temperature controller for the furnace. The reaction apparatus was equipped with four gas mass flowmeters for controlling gas flow rate and a back-pressure valve for regulating the pressure of system. Before the reaction, the hybrid catalyst was activated at 250°C for 4 hrs in pure hydrogen flow. Then synthesis gas was introduced into the reaction system. The hybrid catalysts were evaluated under the condition of 260°C, 2 MPa, and 1875 $ml.h^{-1}.g^{-1}$. CO, CO_2, CH_4 and N_2 were analyzed by a GC equipped with a thermal conductivity detector (TCD), and organic compounds were analyzed by another GC equipped with a flame ionization detector (FID).

3. Catalyst characterization

NH_3-TPD Temperature-programmed desorption of NH_3 (NH_3-TPD) was conducted on an Autochem 2910 instrument (Micromeritics). A 100 mg sample was pre-treated at 500°C for 1 hr and then heated from 100°C to 700°C at a constant rate of 10°C/min after saturation adsorption of NH_3 at 100°C.

Py-IR A pyridine adsorption Fourier-transform Infrared (Py-IR) spectrum was recorded by a Bruker IF113V FTIR spectrometer to study the type of acidity. The IR spectrometer was equipped with an in-situ cell containing CaF_2 windows. In Py-IR experiment, the sample disc was pre-treated under vacuum (1×10^{-3} Pa) at 450°C for 1 hr and then cooled down to room temperature. Subsequently, pyridine was introduced into IR cell at room temperature for 5 minutes to ensure that all acid sites were covered. The sample was heated to 200°C and 350°C respectively at a rate of 10°C/min and the IR spectra was collected at each temperature.

TPO-MS Temperature-programmed oxidation (TPO) was carried out using a quadrupole mass spectrometer OmnistarTM GSD 301 (Pfeiffer Vacuum) for signal collection. A 40 mg sample was heated from ambient temperature to 900°C with a heating rate of 10°C/min under a flow of 5%O_2/95%Ar.

N_2-Physical Absorption N_2 adsorption isotherms were measured by QuadraSorb SI4 instrument at -196°C, Before the N_2 absorption, all the samples were pretreated at 300°C for 5 hrs under vacuum. The total surface area was determined by the BET method while the total pore volume was calculated by the amount of N_2 adsorbed at p/p^0=0.98. The t-plot method was used for the calculation of micropores volume and surface area.

Result and discussion

1. Syngas conversion over different hybrid catalysts

Syngas to hydrocarbon process over a hybrid catalyst of CZA/Pd-zeolite mainly involves the following reactions: (1) the hydrogenation of CO to methanol, (2) the dehydration of methanol to DME, (3) the further dehydration of DME to light olefins, (4) light olefins to final hydrocarbon products, and (5) water-gas shift (WGS) reaction. The relevant reaction equations are as follows.

$$CO + 2H_2 \leftrightarrow CH_3OH \quad (1)$$

$$2CH_3OH \leftrightarrow CH_3OCH_3 + H_2O \quad (2)$$

$$nCH_3OCH_3 \leftrightarrow C_nH_{2n} + nH_2O \quad (3)$$

$$mC_nH_{2n}+pH_2 \leftrightarrow aC_xH_{2x} + bC_yH_{2y+2} + cC_zH_{2y-6} \quad (4)$$

$$CO + H_2O \leftrightarrow CO_2 + H_2 \quad (5)$$

Overall reaction of Equations (1), (2) and (5):

$$3CO + 3H_2 \leftrightarrow CH_3OCH_3 + CO_2 \quad (6)$$

Overall reaction of Equations (1)-(5):

$$3nCO + (3n-p)H_2 \leftrightarrow (1-m)C_nH_{2n} + aC_xH_{2x} + bC_yH_{2y+2} + cC_zH_{2y-6} + 3n/2CO_2 \quad (7)$$

Figure 1 shows the relationship of CO conversion with time on stream (TOS) over different hybrid catalysts. It is observed that the CO conversion over hybrid catalysts is far higher than that over CZA catalyst. This phenomenon is due to the in-situ removal of methanol from methanol/DME dehydration component, which breaks the thermodynamic equilibrium limitation of the methanol synthesis process (Equation 1)[19, 20]. Compared with the other three hybrid catalysts, the CO conversion over CZA/Pdβ was sharply decreased within the primary 60 minutes while the CO conversion over CZA was still stable under the same reaction conditions. The above results indicate that the deactivation of Pdβ leads to the quick deactivation of CZA/Pdβ.

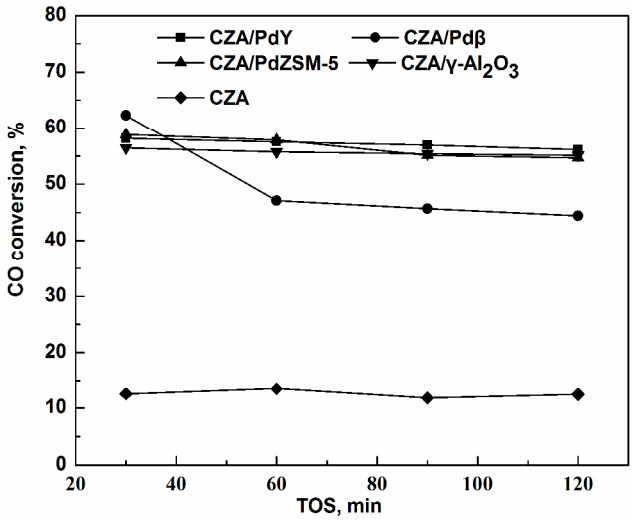

Figure 1. TOS data of CO conversion over different hybrid catalyst. Reaction condition: T=260°C, P=2 MPa, H_2/CO=2, GHSV=1875 $ml.g^{-1}.h^{-1}$.

Table 1 shows the product distribution of syngas conversion over different hybrid catalysts. It is shown that the major product in CZA catalyst was MeOH. Byproducts like hydrocarbons were also formed under the reaction condition. Methanol synthesis process was usually operated at an elevated pressure of 5-10 MPa and temperature of 200-300°C[21]. High reaction temperature and low pressure would lead to a low CO conversion as well as promoting the formation of byproducts. The major product of syngas conversion over CZA/γ-Al_2O_3 became DME and few hydrocarbons were detected in the product. Additionally, plenty of CO_2 was produced. Cu-ZnO based catalyst had great performance for the water gas shift (WGS) reaction (Equation 5)[22]. Methanol formed from CZA catalyst could be dehydrated to

DME on the weak acid sites of γ-Al_2O_3 (Equation 2)[23]. The formed water from the methanol dehydration takes part in the WGS reaction and produces much CO_2. More CO_2 was produced over hybrid catalysts of CZA/Pd-zeolite compared with CZA/γ-Al_2O_3. As we discussed above, water was one of the reactants in the WGS reaction. Compared with syngas conversion over CZA/γ-Al_2O_3, extra water was formed from the further dehydration of DME to hydrocarbons (Equation 3). The extra formed water further promoted the WGS reaction and thus produced more CO_2. The experimental results were also consistent with the overall reaction of syngas to DME process (Equation 4) and syngas to hydrocarbon process (Equation 6). Table 1 shows that little DME and no methanol were detected over the hybrid catalyst of CZA/Pd-zeolite. This was in stark contrast to the product distribution over CZA/γ-Al_2O_3. To further study this phenomenon, we loaded DME synthesis catalyst (CZAA) into the 1st reactor and γ-Al_2O_3 into the 2nd reactor. Thus the feedstock to the 2nd reactor consisted of DME, MeOH, CO_2, unreacted syngas and few hydrocarbons. The major product was still the mixture of DME and methanol (see Table 1). This result showed that γ-Al_2O_3 had great performance for the dehydration of methanol to DME but had little performance for the dehydration of DME to hydrocarbons, which indicated that the active sites for methanol and DME dehydration were different. We think that this difference is related to the surface acidity of the dehydration components.

Table 1. Product distribution of syngas conversion over different hybrid catalysts.

Catalyst bed	Product selectivity, %				
	CO_2	DME	MeOH	EtOH	HCs
CZA	9.9	0.7	83.0	2.2	4.2
CZA/ γ-Al_2O_3[a]	31.8	64.1	3.8	---	0.3
CZA/PdZSM-5	49.2	1.0	---	---	49.9
CZA/Pdβ	47.1	0.8	---	---	52.1
CZA/PdY	48.5	1.0	---	---	50.4
CZAA+γ-Al_2O_3[b]	32.6	62.4	4.4	---	0.7

Reaction condition: T=260°C, P=2 MPa, GHSV=1875 ml.h^{-1}.g^{-1}, TOS=60 min. a. CZA and γ-Al_2O_3 were homogenously mixed with granule type. b. CZAA was loaded in the 1st reactor, T=260°C; γ-Al_2O_3 was loaded in the 2nd reactor, T=260°C, P=2 MPa, H_2/CO=2, GHSV=1875 ml.h^{-1}.g^{-1}, TOS=60 min.

Py-IR data in Table 2 show that only Lewis acid sites existed in γ-Al_2O_3 while Pd modified zeolites had both Brönsted acid sites and Lewis acid sites. The above experimental results suggested that the dehydration of methanol to DME mainly happens on the weak Lewis acid sites while the dehydration of DME to hydrocarbons on the Brönsted acid sites. DME might be one of the intermediate products in the syngas to hydrocarbon process under the existence of Lewis acid sites. Next, DME was further dehydrated to hydrocarbons on neighbouring Brönsted acid sites of Pd modified zeolites.

Table 2. Py-IR data of PdZSM-5, Pdβ, PdY and γ-Al_2O_3.

Catalyst	Acidity(mmol $_{pyridine}$/g $_{catalyst}$)					
	Brönsted acidity(B)		Lewis acidity(L)		B/L	
	200°C	350°C	200°C	350°C	200°C	350°C
PdZSM-5	0.262	0.223	0.058	0.040	4.5	5.6
Pdβ	0.136	0.081	0.125	0.103	1.1	0.8
PdY	0.155	0.118	0.075	0.060	2.1	2.0
γ-Al_2O_3	---	---	0.149	0.062	0.0	0.0

Note: The amount of L and B acidity was calculated from the peak areas at 1446 cm^{-1} and 1548 cm^{-1}. The band at 1548 cm^{-1} corresponds to Brönsted acidity and the band at 1446 cm^{-1} to Lewis acidity.

The hydrocarbon distribution was also different over hybrid catalysts of CZA/Pd-zeolite. As shown in Table 3, a lot of C_4+ hydrocarbons were produced over hybrid catalysts of CZA/PdY and CZA/Pdβ. Over 89% of the C_4 fractions were isobutane. In contrast, plenty of C_2-C_3 paraffins (50%) were produced over CZA/PdZSM-5. Less C_2-C_3 paraffins were found in the hydrocarbon product over CZA/PdY and CZA/Pdβ. This phenomenon was related to the acidity strength and the topology of the Pd modified zeolite. From literature, it was reported that the cracking activity of the catalyst was strongly dependent on the density and strength of the Brönsted acid sites[24]. The strong Brönsted acid promoted the cracking of higher hydrocarbons to lower hydrocarbons. The acid strength and density of different dehydration components were characterized by NH_3-TPD technique. The NH_3 desorption peaks in the temperature ranges of 180-240°C, 260-320°C and 450-600°C are the chemical desorption of NH_3 from weak, medium and strong acid sites, respectively[25]. The peak areas are proportional to the number of the acid sites over the catalyst. As shown in Figure 2, NH_3-TPD spectra mainly shows one peak before 200°C and one peak above 320°C, which is corresponding to the weak acid sites and strong acid sites of catalyst, respectively. PdZSM-5 shows the strongest and has the most acid sites among the dehydration catalysts while γ-Al_2O_3 shows the weakest and least ones. From Table 2 we know that the strong acid sites in PdZSM-5 were mainly Brönsted acid sites. The result indicates that the high content of C_2-C_3 paraffins over CZA/PdZSM-5 may come from the cracking of higher hydrocarbons on strong Brönsted acid sites of PdZSM-5.

Table 3. Effect of zeolite topology on hydrocarbon distribution.

Catalyst bed	Product distribution in Hydrocarbon, %					Iso-C_4/C_4,%
	C_1	C_2	C_3	C_4	C_5-C_{12}	
CZA/PdZSM-5	2.4	20.8	29.2	16.5	31.0	65.4
CZA/Pdβ	0.5	2.8	9.6	46.6	40.5	90.2
CZA/PdY	0.9	10.4	11.8	54.5	22.3	89.1

Reaction condition: T=260°C, P=2 MPa, H_2/CO=2, GHSV=1875 ml.h^{-1}.g^{-1}, TOS=60 min.

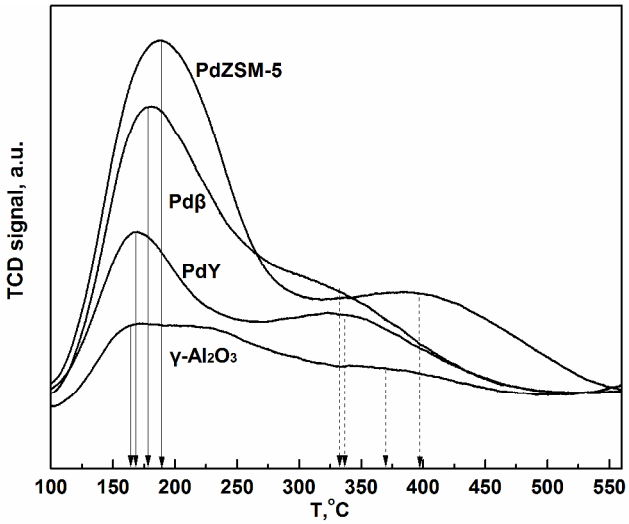

Figure 2. NH_3-TPD spectrum of different catalyst PdZSM-5, Pdβ, PdY and γ-Al_2O_3

Figure 3 shows the carbon number distribution of C_5-C_{12} hydrocarbons over the three different hybrid catalysts. Few C_{11}-C_{12} hydrocarbons were detected over CZA/PdZSM-5 and CZA/PdY. Meanwhile, about 26% C_{11}-C_{12} hydrocarbons were detected over the CZA/Pd-β catalyst. It is noteworthy that almost all the C_{11}-C_{12} hydrocarbons were hexamethylbenzene. This phenomenon has close correlation with the topology of different Pd zeolites.

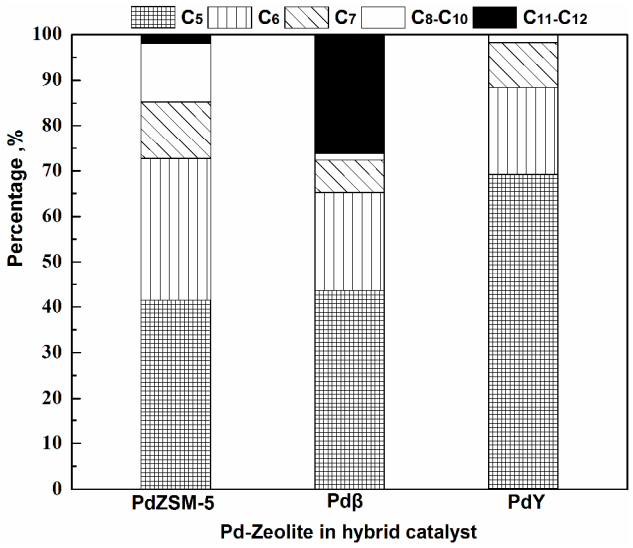

Figure 3. Percentage of different fractions in C_5-C_{12} hydrocarbon. Reaction conditions: 260°C, 2 MPa, $H_2/CO=2$, GHSV=1875 $ml.h^{-1}.g^{-1}$. Note: about 100% C_{11}-C_{12} hydrocarbons over CZA/Pdβ catalyst is hexamethylbenzene.

Table 4 gives detailed information about the topology of zeolite HZSM-5, Hβ and HY. Both Hβ and HY possess a cavity with different sizes compared with HZSM-5. The pore size order of the three zeolites is as follows: HZSM-5<Hβ<HY. Compared with PdZSM-5, it was much easier for produced methanol and DME to enter the channel of PdY and Pdβ due to their larger channel openings. The large pore and cavity of Pdβ and PdY could provide more space for chain growth reactions like oligomerization. DME was dehydrated to lower olefins and converted into higher hydrocarbons such as C_5+ olefins, aliphatic hydrocarbons, naphthenes and aromatics by oligomerization, cyclization and aromatization on PdY and Pdβ. However, the detected C_5-C_{12} hydrocarbons over the CZA/PdY catalyst were the least among the three hybrid catalysts. A similar phenomenon was also found by Fujimoto et al[6]. The large pore in HY was considered to enhance the mass transfer of both reactants and products, which would shorten the residence time of lower olefins in the channels of HY and weaken the oligomerization reactions. Note that hydrocarbons in C_5-C_{12} over the above three hybrid catalysts are mainly gasoline-type branched paraffins (see Figure 4).

Table 4. The structure parameters of zeolite HZSM-5, Hβ and HY.

Zeolite type	Framework type	Ring size (T-atoms)	Pore size/nm	Channel system	Cavity size/ nm
HZSM-5	MFI	10, 6, 5, 4	0.53×0.56	3 D	none
Hβ	BEA	12, 6, 5, 4	0.67×0.66	3D	~1nm
HY	FAU	12, 6, 4	0.74×0.74	3D	~1.3nm

Note: Data are from IZA.

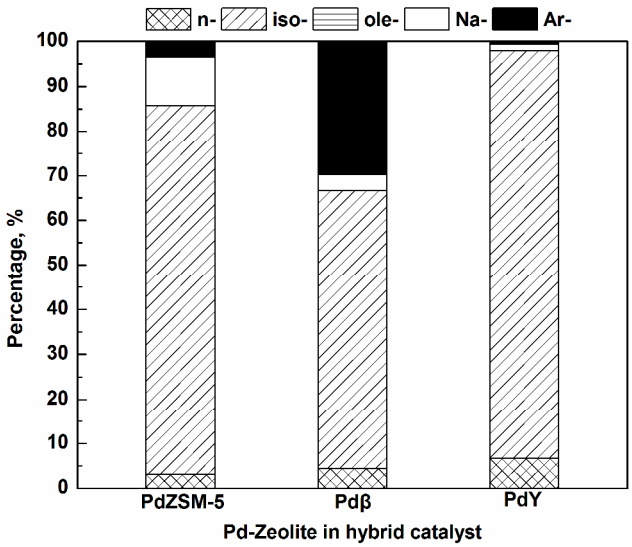

Figure 4. Compositions in C_5-C_{12} fractions. Note: n-: n-paraffin; iso-: iso-paraffin; ole-: olefins; Na-naphthene; Ar- aromatics. Reaction conditions: 260°C, 2 MPa, $H_2/CO=2$, GHSV=1875 $ml.h^{-1}.g^{-1}$.

2. Catalyst deactivation analysis

Catalyst deactivation by coke is one of the main problems in the field of catalytic reactions[26]. M. Guisnet et al thought that the formation of coke had close correlation with the topology of the zeolite[27-29]: (i) pore size (ii) existence or non-existence of cavities and (iii) the diffusion of the reactants and/or the products in zeolite. Additionally, the density of Brönsted acid and Lewis acid also influences coke formation over zeolite catalyst. From the discussion of 3.1, we know that the deactivation of Pdβ leads to the quick deactivation of the hybrid catalyst of CZA/Pdβ. To understand the reason for the deactivation of the hybrid catalysts

for syngas conversion, TPO-MS and N_2 physical adsorption techniques had been carried out.

Table 5a Textural properties of Pd zeolite and spent Pd zeolite

Sample	V_{pore} ($cm^3.\ g^{-1}$)[a]	V_{micro} ($cm^3.\ g^{-1}$)[b]	S_{micro} ($m^2.\ g^{-1}$)[b]	S_{BET} ($m^2.\ g^{-1}$)[c]	$S_{External}$ ($m^2.\ g^{-1}$)[c]
PdZSM-5	0.215	0.133	326.9	378.3	51.4
PdZSM-5-S	0.199	0.107	265.0	308.0	43.0
Pdβ	0.555	0.140	350.9	529.2	178.3
Pdβ-S	0.489	0.090	220.0	395.1	175.0
PdY	0.478	0.276	610.3	709.1	98.9
PdY-S	0.388	0.204	491.5	590.6	99.1

a. Measured Vads at $p/p^0 = 0.98$.
b. t-plot method.
c. BET method.
"S" means "spent"

Table 5b The reduction rate of physical properties in spent Pd modified zeolite

Sample	dV_{pore}/V_{pore},%	dV_{micro}/V_{micro},%	dS_{micro}/S_{micro},%	dS_{BET}/S_{BET},%	$dS_{External}/S_{External}$, %
PdZSM-5-S	7.4	19.5	18.9	18.6	16.3
Pdβ-S	11.9	35.7	37.3	25.3	1.9
PdY-S	18.8	26.1	19.5	16.7	~0

Note: $dX/X=(X_0-X_i)/X_0$, which means the reduction rate of the samples' physical properties. X_0 means the property value of fresh catalyst; Xi means the property value of spent catalyst.

As shown in Figure 5, obvious CO_2 and H_2O signals were detected by mass spectrometer (MS) in the three spent Pd modified zeolites (PdZSM-5-S, Pdβ-S and PdY-S), especially in Pdβ-S and PdY-S. Only the weakest H_2O and CO_2 signals were detected over PdZSM-5-S which was consistent with good stability of CZA/PdZSM-5. TPO-MS data shows three CO_2 peaks for PdZSM-5-S while two peaks for both Pdβ-S and PdY-S. N_2 physical adsorption data (see Table 5a) show that the total pore volume of the three spent Pd-zeolites is decreased. The order of reduced volume is PdZSM-5-S < Pdβ-S < PdY-S which is in line with the results of TPO-MS. Table 5b shows that the reduction rate order of external surface is PdY-S < Pdβ-S < PdZSM-5-S. In contrast, the reduction rate order of volume is PdZSM-5-S < Pdβ-S < PdY-S. The results of TPO-MS and N_2 physical adsorption techniques indicate that external coke was formed over PdZSM-5, while higher hydrocarbons were formed within the micropores of Pdβ and PdY during syngas conversion reactions. These trapped higher hydrocarbons became carbonaceous compounds and blocked the pores, especially micropores, of Pd-zeolites. The first peak at about 300°C belongs to the calcinations of external coke while peaks greater than 400°C belong to the calcinations of internal coke. Table 3 shows that both Hβ and HY contain a 12-ring opening channel system and a cavity while HZSM-5 contains a 10-ring opening channel system but no cavity. The pore sizes of the three Pd-zeolites are 0.53×0.56 nm for PdZSM-5, 0.67×0.66 nm for Pdβ and 0.74×0.74 nm for PdY, respectively. The large cavity of PdY (1.3 nm) and Pdβ (1.0 nm) can provide a much bigger space for the following chain growth reactions to form higher hydrocarbons like polymethylbenzene. Many hexamethylbenzene were detected over CZA/Pdβ. From the literature, we know that the kinetic diameter of hexamethylbenzene is approximately 0.72 nm[30], which is bigger than the pore size of Pdβ. The formation of hexamethylbenzene should happen in the cavity of Pdβ. As the chemical bond in zeolite framework is elastic and vibrational[31], the hexamethylbenzene could also diffuse out from the large pores of Pdβ. That's why we detected hexamethylbenzene over CZA/Pdβ. The cavity size of Pdβ (~ 1.0 nm) is smaller than the cavity size of PdY (~1.3 nm). The maximal size of hydrocarbons formed in the cavities of PdY should be larger than that formed in the cavities of Pdβ. Thus, the formed hydrocarbons in the cavities of PdY might be higher aromatics with 2-ring and 3-ring (Polycyclic aromatic hydrocarbons, PAHs). The formed higher aromatics in cavities were trapped into the pores of zeolites which become the precursors of coke. For PdZSM-5, the chain growth reactions were limited for its narrow pore size. The formation of higher aromatics was restrained in PdZSM-5. However, there were also carbonaceous compounds deposited over the external surface of PdZSM-5. In general, the blockage of micropores by hydrocarbon-type coke caused the deactivation of hybrid catalysts.

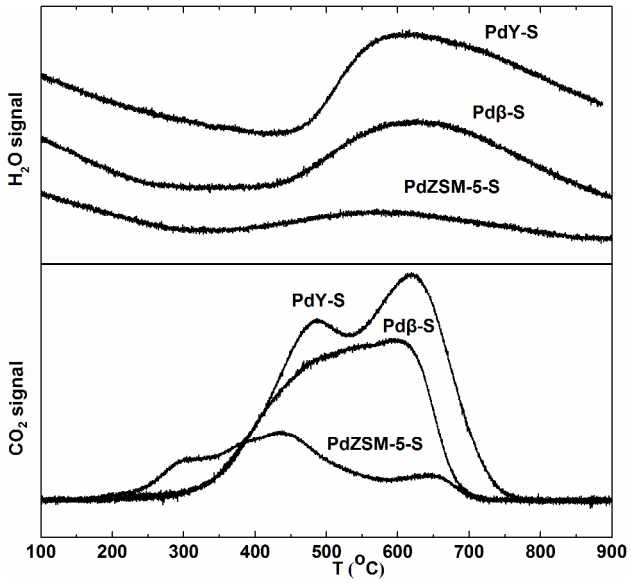

Figure 5. TPO-MS spectrum of spent PdZSM-5-S, Pdβ-S and PdY-S zeolite.

Conclusion

Synthesis gas could be converted into different hydrocarbon fractions over hybrid catalyst composed of Cu-ZnO-Al_2O_3 methanol synthesis catalyst and Pd modified zeolite. The results indicate that the intermediate step of DME dehydration to hydrocarbons mainly happened on the Brönsted acid sites while methanol could be effectively converted into DME on the weak Lewis acid sites. Additionally, hydrocarbon distribution and carbonaceous compound formation had a close relationship with the topology and the acidity of Pd modified zeolite. More C_4+ hydrocarbons were formed over hybrid catalyst of CZA/Pd-β and CZA/Pd-Y due to their large pore and cavities. However, the cavity also provided enough space for the formation of higher

aromatics which would block the micropores of Pd modified zeolite in hybrid catalyst and cause the activity loss of the hybrid catalyst. For CZA/PdZSM-5, the formation of higher aromatics was restrained because of the narrow pores in PdZSM-5. Carbonaceous compounds were deposited on the external surface of PdZSM-5 because of its strongest acid sites. The compositions of C_5-C_{12} were rich in gasoline-type branched paraffins. There is still much work left to increase the content of liquid fuels in hydrocarbon products over a hybrid catalyst, improve the stability of the hybrid catalyst and promote the efficiency of carbon conversion into hydrocarbons.

Acknowledgements

The authors gratefully acknowledge the financial support from BP Company through BP's Energy Innovation Laboratory at the Dalian Institute of Chemical Physics, CAS. Thanks for the helpful discussion of Prof. Yanxin Chen.

Notes and references

[a] *Dalian National Laboratory for Clean Energy, Dalian Institute of Chemical Physics, Chinese Academy of Sciences, Dalian 116023, Liaoning, China.*
[b] *University of Chinese Academy of Sciences, Beijing 100039, China.*
Corresponding authors:
Fax: 86-411-84379152; Tel: 86-411-84379229; E-mail: geqj@dicp.ac.cn.
Fax: 86-411-84581234; Tel: 86-411-84581234; E-mail: xuhy@dicp.ac.cn.

† Electronic Supplementary Information (ESI) available: [details of any supplementary information available should be included here]. See DOI: 10.1039/b000000x/

‡ Footnotes should appear here. These might include comments relevant to but not central to the matter under discussion, limited experimental and spectral data, and crystallographic data.

1. W. Maqbool and E. S. Lee, *Chem. Eng. Technol.,* 2014, **37**, 995-1001.
2. J. R. Rostrup-Nielsen, *Catal. Today*, 2002, **71**, 243-247.
3. P. Tunå and C. Hulteberg, *Fuel*, 2014, **117**, Part B, 1020-1026.
4. N. Tsubaki, Y. Yoneyama, K. Michiki and K. Fujimoto, *Catal. Commun.*, 2003, **4**, 108-111.
5. H. M. Torres Galvis, J. H. Bitter, C. B. Khare, M. Ruitenbeek, A. I. Dugulan and K. P. de Jong, *Science*, 2012, **335**, 835-838.
6. K. Fujimoto, H. Saima and H.-o. Tominaga, *Bull. Chem. Soc. Jpn.*, 1985, **58**, 3059-3060.
7. N. V. Kolesnichenko, L. E. Kitaev, Z. M. Bukina, N. A. Markova, V. V. Yushchenko, O. V. Yashina, G. I. Lin and A. Y. Rozovskii, *Kinet. Catal.*, 2007, **48**, 789-793.
8. C. Wang, D. Zhang, C. Fang, Q. Ge and H. Xu, *Fue*l, 2014, **134**, 11-16.
9. Q. Zhang, K. Cheng, J. Kang, W. Deng and Y. Wang, *ChemSusChem*, 2014, **7**, 1251-1264.
10. J. Sun, C. Xing, H. Xu, F. Meng, Y. Yoneyama and N. Tsubaki, *J. Mater. Chem. A,* 2013, **1**, 5670-5678.
11. J. Kang, K. Cheng, L. Zhang, Q. Zhang, J. Ding, W. Hua, Y. Lou, Q. Zhai and Y. Wang, *Angew. Chem.*, 2011, **123**, 5306-5309.
12. S. Sartipi, K. Parashar, M. Makkee, J. Gascon and F. Kapteijn, *Catal. Sci. Technol.*, 2013, **3**, 572-575.
13. R. A. Dagle, J. A. Lizarazo-Adarme, V. Lebarbier Dagle, M. J. Gray, J. F. White, D. L. King and D. R. Palo, *Fuel Process. Technol.,* 2014, **123**, 65-74.
14. X. Ma, Q. Ge, C. Fang, J. Ma and H. Xu, Fuel, 2011, **90**, 2051-2054.
15. K. Fujimoto, *J Jan. Petrol. Inst.,* 2004, **47**, 394-402.
16. Q. Ge, Y. Lian, X. Yuan, X. Li and K. Fujimoto, *Catal. Commun.*, 2008, **9**, 256-261.
17. C. D. Chang, W. H. Lang and A. J. Silvestri, *J. Catal.,* 1979, **56**, 268-273.
18. T. Ma, H. Imai, Y. Suehiro, C. Chen, T. Kimura, S. Asaoka and X. Li, *Catal. Today,* 2014, **228**, 167-174.
19. J. G. van Bennekom, R. H. Venderbosch, J. G. M. Winkelman, E. Wilbers, D. Assink, K. P. J. Lemmens and H. J. Heeres, *Chem. Eng. Sci.,* 2013, **87**, 204-208.
20. T. Ogawa, N. Inoue, T. Shikada and Y. Ohno, *J. Nat. Gas Chem.,* 2003, **12**, 219-227.
21. M. Behrens, F. Studt, I. Kasatkin, S. Kühl, M. Hävecker, F. Abild-Pedersen, S. Zander, F. Girgsdies, P. Kurr, B.-L. Kniep, M. Tovar, R. W. Fischer, J. K. Nørskov and R. Schlögl, *Science,* 2012, **336**, 893-897.
22. K. M. V. Bussche and G. F. Froment, *J. Catal.,* 1996, **161**, 1-10.
23. M. Xu, J. H. Lunsford, D. W. Goodman and A. Bhattacharyya, *Appl. Catal. A,* 1997, **149**, 289-301.
24. M. Niwa, K. Suzuki, N. Morishita, G. Sastre, K. Okumura and N. Katada, *Catal. Sci. Technol.*, 2013, **3**, 1919-1927.
25. S. Fathi, M. Sohrabi and C. Falamaki, *Fuel*, 2014, **116**, 529-537.
26. M. Guisnet, *J. Mol. Catal. A: Chem.,* 2002, **182**, 367-382.
27. M. Guisnet and P. Magnoux, *Appl. Catal.,* 1989, **54**, 1-27.
28. B. Paweewan, P. J. Barrie and L. F. Gladden, *Appl. Catal. A,* 1999, **185**, 259-268.
29. M. Guisnet, L. Costa and F. R. Ribeiro, *J. Mol. Catal. A: Chem.*, 2009, **305**, 69-83.
30. Q. Zhu, J. N. Kondo, T. Tatsumi, S. Inagaki, R. Ohnuma, Y. Kubota, Y. Shimodaira, H. Kobayashi and K. Domen, *J. Phys. Chem. C*, 2007, **111**, 5409-5415.
31. Liu Yi and G. Zi, *Acta Petrolei Sinica(Petroleum Processing Section)*, 1996, **12**, 35-40.

